Large Andreev bound state zero-bias peaks in a weakly dissipative environment

Zhichuan Wang,[1,2,3,*] Shan Zhang,[2,*] Dong Pan [ORCID],[4,*] Gu Zhang,[5,*] Zezhou Xia,[2] Zonglin Li,[2] Donghao Liu [ORCID],[2] Zhan Cao,[5]
Lei Liu,[4] Lianjun Wen,[4] Dunyuan Liao,[4] Ran Zhuo,[4] Yongqing Li,[1,3] Dong E. Liu,[2,5,6] Runan Shang,[5,†]
Jianhua Zhao [ORCID],[4,‡] and Hao Zhang [ORCID][2,5,6,§]

[1]*Beijing National Laboratory for Condensed Matter Physics, Institute of Physics, Chinese Academy of Sciences, Beijing 100190, China*
[2]*State Key Laboratory of Low Dimensional Quantum Physics, Department of Physics, Tsinghua University, Beijing 100084, China*
[3]*School of Physical Sciences, University of Chinese Academy of Sciences, Beijing 100049, China*
[4]*State Key Laboratory of Superlattices and Microstructures, Institute of Semiconductors, Chinese Academy of Sciences,*
P.O. Box 912, Beijing 100083, China
[5]*Beijing Academy of Quantum Information Sciences, Beijing 100193, China*
[6]*Frontier Science Center for Quantum Information, Beijing 100084, China*

The detection of Majorana zero modes still remains elusive after extensive searches. The current debates focus on the experimental observation of large zero-bias peaks (ZBPs) near $2e^2/h$ in tunneling conductance. These large ZBPs, induced by Andreev bound states, mimic the Majorana signature and suggest that new diagnostic tools or experimental knobs are highly desired. In this paper, we introduce an interaction effect on these large ZBPs using a weakly dissipative probe. By increasing temperature (T), we establish that these large ZBPs can reveal a zero-bias conductance increase, a non-Fermi-liquid behavior due to the environmental Coulomb blockade. This observation forms a sharp contrast to nondissipative devices where ZBPs follow a Fermi-liquid T dependence. Our results open prospects for a better understanding of large ZBPs induced by Andreev bound states and hold relevance for future Majorana detection.

I. INTRODUCTION

Andreev bound states (ABSs) can emerge in nonuniform superconductors by Andreev scatterings at energies below the superconducting gap [1,2]. Hybrid semiconductor-superconductor systems [3–6] provide an ideal test bed to study these subgap states, owing to the proximity effect mediated by Andreev reflections and the high tunability of carrier density using electrostatic gates. Fascinating physics can be revealed by adding additional elements, e.g., one dimensionality and spin-orbit coupling [7–12]. These hybrid nanowires, with the semiconductors being InAs or InSb, are further predicted to host Majorana zero modes (MZMs) [13,14] where one ABS can be spatially separated into two "halves" (MZMs). In tunneling conductance, zero-bias peaks (ZBPs) can be observed [8,15–22] as a possible signature for MZMs as well as zero-energy ABSs. The similarities between ABSs and MZMs, e.g., large ZBPs on the order of $2e^2/h$ for both cases, create huge debates on distinguishing them [23–35].

Recently, motivated by a theoretical work [36], we have added a resistive lead as a strongly dissipative environment to hybrid InAs-Al devices [37]. Previously, dissipative tunnelings of metallic junctions [38–42] and semiconductor nanostructures [43–49] have been widely studied which

exhibit the dynamical or environmental Coulomb blockade (ECB) with power laws emulating Luttinger liquid physics [50]. Here (see also Ref. [37]), the interaction effect in the environment acts on the InAs-Al nanowire junction where ABSs emerge. Different from how the conventional ECB works, dissipative tunneling is mediated by Andreev reflection and into a discrete subgap state. Reference [36] predicts that this dissipative environment could identify topological ZBPs by suppressing the trivial ones. In the strongly dissipative regime, we have shown that most zero-energy ABSs are revealed as split peaks instead of ZBPs [37]. However, large ZBPs near $2e^2/h$, the core of current debates [32–34], still remain to be explored by a dissipative probe. To reveal large ZBPs, in this paper we lower the probing lead resistance from ~5.7 kΩ in Ref. [37] to ~2.7 kΩ. We show that ABS-induced ZBPs are not fully suppressed down to the lowest accessible temperature; therefore, we shall refer to this regime as a "weak dissipation" one. The large ZBPs near $2e^2/h$ follow a unique temperature dependence dramatically different from that of small ZBPs or ZBPs in regular devices without dissipation. We ascribe this difference to the dynamical competition between ECB and thermal averaging. Our result suggests that the dissipation strength reported in this paper is not enough to fully suppress ABS-induced ZBPs at the current fridge temperature.

II. EXPERIMENTAL RESULTS

Figure 1(a) shows the scanning electron micrograph (SEM) of device A. An InAs nanowire (gray) with a thin Al shell

*These authors contributed equally to this work.

†shangrn@baqis.ac.cn

‡jhzhao@semi.ac.cn
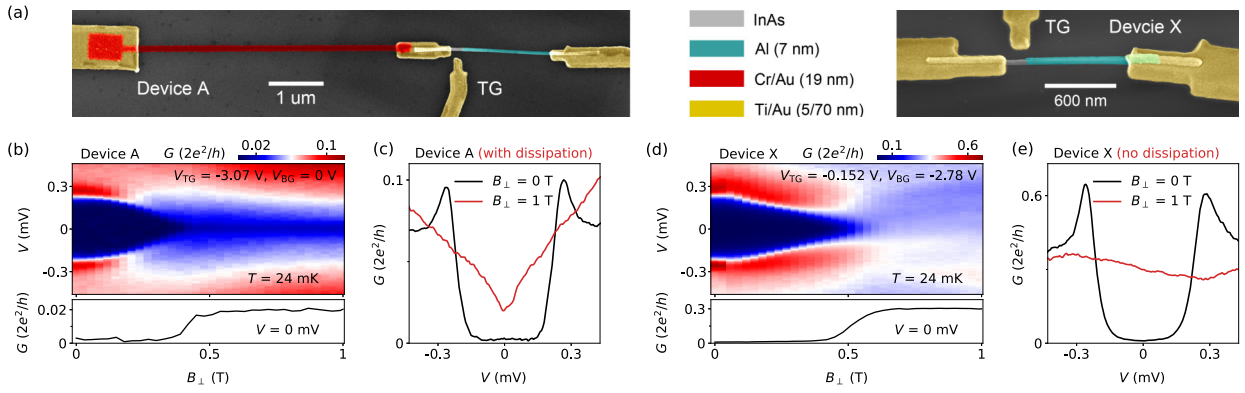
§hzquantum@mail.tsinghua.edu.cn

FIG. 1. (a) False-color SEMs of device A (left) and control device X (right). See labeling for Al, Cr/Au, and Ti/Au film thickness. The Al shells on InAs are half coverage, and for visibility, the InAs front facets are false colored. Device X is the same device used in Ref. [37]. (b) B scan of the superconducting gap in device A. B is in plane and perpendicular to the wire axis. Lower panel: Zero-bias line cut. (c) Line cuts from (b) at 0 and 1 T. (d), (e) B scan of the gap in device X. $T \sim 24$ mK.

(cyan) is first contacted by Ti/Au (yellow), and then connected to a resistive film (red), serving as the dissipative environment. Resistance of the dissipative film is designed and later estimated to be $\sim$2.7 kΩ [see Fig. S1 in the Supplemental Material (SM) [51] for details]. The device can be tuned by a side tunnel gate (TG) and a global back gate (BG) which is p-doped Si covered by 300-nm-thick SiO$_2$. Growth and transport details of these hybrid InAs-Al nanowires can be found in Refs. [19,52]. We apply a total bias voltage (V_{bias}) on the left Ti/Au lead, and measure the current I from the right contact. The bias drop on the InAs-Al part is $V = V_{\text{bias}} - I \times R_{\text{series}}$, where $R_{\text{series}} = R_{\text{filters}} + R_{\text{film}}$ includes resistance of the fridge filters and the dissipative film, both estimated based on independent calibration. The device differential conductance, $G \equiv dI/dV = (dV_{\text{bias}}/dI - R_{\text{series}})^{-1}$, has R_{series} excluded.

In Fig. 1(b) we tune the device into the tunneling regime and resolve the superconducting gap (see Fig. S2 in SM [51] for the gate scan). The gap is closed by a magnetic field (B), perpendicular to the nanowire, at $\sim$0.5 T. After the gap closing, a dip is resolved near zero bias [red curve in Fig. 1(c)]. This suppression of G near zero bias (see Fig. S3 in SM [51] for more scans) is a signature of ECB. We further quantify this suppression with a power law and find rough matches (see Fig. S4 in SM [51]). In our control device X, an InAs-Al nanowire without the dissipative resistor, G is usually flat after the gap closing without noticeable features near zero bias as shown in Figs. 1(d) and 1(e) (see Ref. [37] for more characterizations of device X at different barrier transmissions).

We now align B parallel to the nanowire and find large ZBPs (Fig. 2) due to zero-energy ABSs. Note the different barrier transparencies (reflected by the outside-gap conductance) between Fig. 1 (the tunneling regime) and Fig. 2 (more opened regime), corresponding to different gate voltages. Figure 2(a) shows a B scan of an ABS, likely disorder induced, in device B at temperatures (T) of 24 and 240 mK. T refers to the fridge T unless specified. Device B has a dissipative resistor ($\sim$2.7 kΩ) similar to that in device A. At 0.96 T, two peaks merge at zero and form a large ZBP with height exceeding $2e^2/h$ [see Fig. 2(b) for line cuts]. Interestingly, the ZBP height at an elevated T of 240 mK (red) is higher than that at base T of 24 mK (black). This unusual T dependence

is qualitatively different from those in nondissipative devices where the ZBP height always decreases as T increases, a purely thermal broadening (averaging) effect (see Fig. S5 in SM [51] for examples in the control device X). We attribute this unusual T dependence to the mixing or competing effect of ECB and thermal broadening. ECB suppresses zero-bias G (the ZBP height) at low T (24 mK). Higher T (240 mK) diminishes ECB and enhances the height. On the contrary, thermal broadening, an averaging effect over a peak, leads to the opposite trend in T dependence. For large and broad ZBPs, the thermal broadening effect is not obvious at low T, therefore ECB may dominate the trend in T dependence, as visualized by the difference between the black and the red curves in Fig. 2(b). Note that ECB is the strongest near $V = 0$.

To simulate the thermal broadening effect, we use the formula $G(V, T) = \int_{-\infty}^{+\infty} G(\epsilon, 0) \frac{\partial f[e(V-\epsilon), T]}{\partial \epsilon} d\epsilon$, where $f(E, T) = \frac{1}{e^{E/k_B T} + 1}$ is the Fermi distribution function. $G(V, T)$ at high T can be calculated by this convolution using $G(V, T = 0$ K) as an input which we replace with $G(V, T = 24$ mK). This assumption should be valid for T much larger than 24 mK. The red dashed lines in Fig. 2(a) (lower panel) and Fig. 2(b) are the simulation results for $T = 240$ mK, noticeably lower than the measured G at the same T (red lines). This deviation suggests that thermal broadening is not the only effect and ECB should be included in the T dependence of large ZBPs.

Figure 2(c) shows the gate dependence of the large ZBP where again a sizable deviation can be found between the measurement (red line) and the thermal simulation (dashed line) for $T = 239$ mK. Figure 2(d) shows a line cut of the near-zero-energy ABS: split peaks at 24 mK evolving into a large ZBP at 239 mK. The red dashed line is the thermal simulation which could also merge split peaks into a ZBP but at a cost of lowering the peak height.

ECB not only suppresses the ZBP height, but also modifies the peak shape due to its nonuniform suppression on G over bias. In Fig. 2(e), the large ZBP at base T shows a larger deviation from the Lorentzian fit (dashed line) than that at higher T. This phenomenon is expected since ECB is stronger (weaker) at lower (higher) T. Figure 2(f) shows the full T dependence of the zero-bias G (black dots) for this ZBP. The black dashed
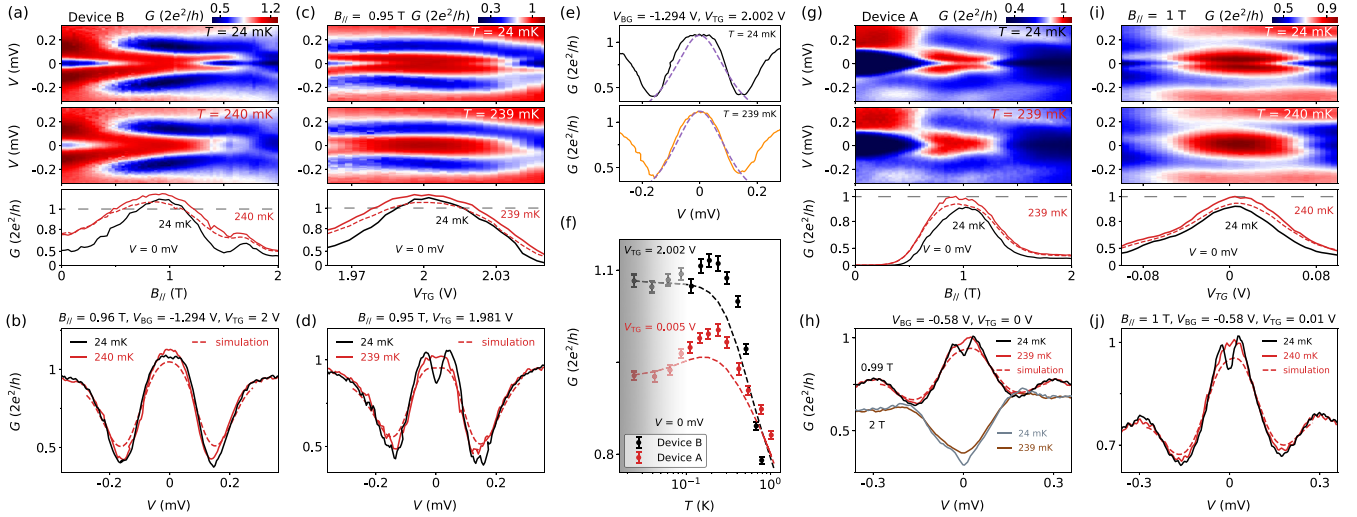
FIG. 2. (a) G vs V and B at $T = 24$ mK (upper) and 240 mK (middle) for device B. Lower panel: Zero-bias line cuts, and thermal simulation for $T = 240$ mK (red dashed line). (b) Line cuts from (a) at $B = 0.96$ T and thermal simulation (dashed line) for 240 mK. (c) V_{TG} scan at $B = 0.95$ T for 24 mK (upper) and 239 mK (middle). Lower panel: Zero-bias line cuts and thermal simulation (dashed line). (d) Line cuts from (c) and thermal simulation (dashed line) for 239 mK. (e) A ZBP line cut from (c) at 24 mK (upper) and 239 mK (lower). Dashed lines are the Lorentzian fits assuming 24 and 239 mK thermal broadening. (f) T dependence of zero-bias G. The dashed line is the thermal simulation. Black for device B and red for device A from (g)–(j). (g)–(j) Similar to (a)–(d) but for device A. In the lower panels of (a), (c), (g), and (i), the y axis is linearly scaled for G^2 instead of G, to better resolve the deviations at higher G's.

line is the thermal simulation which, as expected, shows a monotonic decrease with increasing T. Contrarily, the measured ZBP height first increases (ECB being weakened) and then decreases until T is too high where thermal broadening starts dominating. We sketch a gradient gray background for $T < 100$ mK to indicate that below 100 mK the electron T gradually deviates from the fridge T and finally saturates. Since we focus on the T dependence from 100 to 400 mK, the conclusion should not be affected by this saturation of electron T.

Similar ZBPs near $2e^2/h$ (with a smaller above-background peak height) can also be observed in device A, as shown in Figs. 2(g)–2(j). This zero-energy ABS resolves a small splitting at base T [black curves in Figs. 2(h) and 2(j)]. This ZBP with a splitting feature has no fundamental difference from the large ZBP in Fig. 2(b) (black curve): If a lower temperature could be reached in Fig. 2(b), the ZBP there would also split. Splitting or not depends on the zero-energy ABS details, dissipation strength, and T. If the dissipation strength was increased more, most zero-energy ABS-induced ZBPs would also split. In fact, in Fig. 2(a) (for B slightly different from 0.96 T) and Fig. 2(d), we could also find large ZBPs at higher T's which resolve a small splitting at base T. The main noticeable difference between base T (black curve) and higher T (red curve) in Figs. 2(h) and 2(j) is the "triangle" area near zero bias, a visualization of ECB (also visible for the line cuts at 2 T). Note that thermal simulation (red dashed lines) conserves the area underneath the curve, making the peak height lower and peak width wider for higher T's.

The red dots in Fig. 2(f) illustrate the T evolution of the zero-bias G corresponding to this zero-energy ABS. With increasing T, the zero-bias G first increases and then decreases, similar to the black dots, though if using a curve of a split peak

at base T as the input, thermal simulation would also give an initial increase of G (purely due to the averaging effect on a dip) as shown by the red dashed line. This increase is much less than the measurement data, indicating the noticeable role of ECB. For more T dependence of the ABSs in Fig. 2, see Fig. S6 in SM [51].

Above we have demonstrated the interplay between weak dissipation (ECB) and thermal broadening on large ZBPs induced by zero-energy ABSs. These large ZBPs generally have a large peak width, and are therefore immune to thermal broadening for T's being not too high (e.g., below 300 mK). Within this range, increasing T diminishes ECB and enhances the zero-bias G, causing deviations from the Fermi-liquid T dependence. Figure 2 corresponds to high barrier transparencies, reflected by the outside gap conductance ($\sim$0.7–0.9 × $2e^2/h$). Since high transparency may weaken the ECB [43], in Figs. S4(a) and S4(g) [51] we show that ECB suppression is still present at transparencies similar to the ones in Fig. 2.

In Fig. 3 we study small ZBPs in device A under the same dissipation strength. Figures 3(a) and 3(b) show the B and gate scans of an ABS at base T. The level crossing point, corresponding to a zero-energy ABS, resolves a small ZBP (peak height $\sim$0.3 × $2e^2/h$). The ZBP width is also narrower than those in Fig. 2, and therefore it is more sensitive to thermal averaging. Indeed, in Fig. 3(b) (lower panel), the thermal simulation (dashed line) for $T = 223$ mK agrees reasonably well with the measurement (red line), suggesting that thermal broadening is the dominating effect, different from the case in Fig. 2.

Figures 3(c) and 3(d) show the full T evolution of this small ZBP. The zero-bias G [dots in Fig. 3(d)] shows a monotonic decrease as increasing T, qualitatively different from the trend of T dependence in Fig. 2. Moreover, thermal
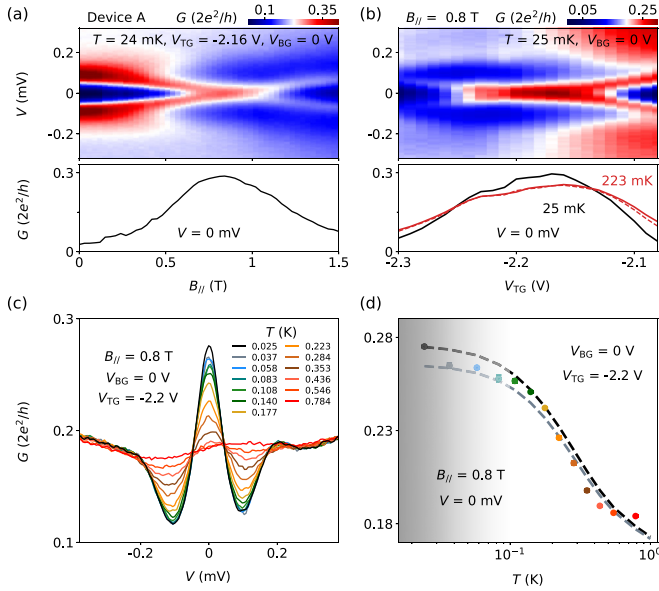
FIG. 3. (a) *B* dependence of a small ZBP in device A at 24 mK. Lower panel: Zero-bias line cut. (b) V_{TG} scan of this ZBP at $B = 0.8$ T. $T = 25$ mK. Lower panel: Zero-bias line cuts at 25 mK (black) and 223 mK (red curve), together with thermal simulation (red dashed line). (c) *T* dependence of the ZBP. (d) Zero-bias *G* (dots) from (c). The black and gray dashed lines are thermal simulations using the 25- and 37-mK data as the input for $G(V, 0)$, respectively, to account for possible instabilities during measurement.

simulation [both black and gray dashed lines in Fig. 3(d)] matches reasonable well with the measurement, confirming thermal averaging as the dominating effect for small ZBPs. Note that weak dissipation should still be present for this ABS since they all share the same dissipative resistor. The narrower peak widths for small ZBPs make them more sensitive to thermal averaging. This causes the ECB effect to be almost unnoticeable in the *T* evolution unless lower temperatures could be reached. For more *T* dependence and gate scans of this ABS, see Fig. S7 in SM [51]. In Fig. S8, we present some stability tests of the ABSs in Figs. 2 and 3 to rule out possible gate shifts or charge jumps. Figures S9 and S10 in SM [51] show four more zero-energy ABSs with intermediate ZBP heights to illustrate the gradual transition from large to small ZBPs.

III. THEORETICAL CALCULATIONS

In Fig. 4, we present the result of the renormalization group (RG) calculation for zero-energy ABSs by fixing the dissipation strength $r = 0.1$. This *r* translates to an effective dissipative resistance of $r \times h/e^2 \sim 2.58$ kΩ, similar to the cases of devices A and B. In the theory model [53], we could modify the lead-ABS tunnel couplings for electrons (t_e) and Andreev reflected holes (t_h) to realize different ZBP heights: If t_e and t_h are larger and closer, the ZBP height is larger. Figure 4 demonstrates the *T* dependence of zero-energy ABSs with different heights (colors). When *T* decreases toward absolute zero, the zero-bias *G* should be suppressed toward zero due to dissipation for all ABS cases, causing the ZBP splitting. When *T* is high enough and increases, ECB is diminished and
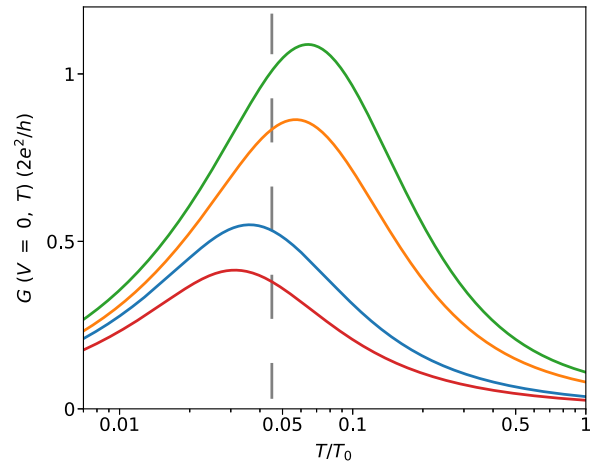

FIG. 4. Renormalization group (RG) calculation of *G* for various zero-energy ABSs (different colors), corresponding to different ZBP heights. The dissipation strength $r = 0.1$ for all curves. T_0 refers to the starting RG temperature. We assign the base *T* in experiment to the vertical dashed line.

the ZBP is thermally smeared, also causing the zero-bias *G* to decrease. These two regions combined together form the shape of *T* dependence in Fig. 4 with a maximum peak at an intermediate *T*. The key point is that this intermediate *T* is different for large and small ZBPs. By comparing with experimental data, we think our base *T* likely corresponds to the vertical dashed line. Under this assumption, for small ZBPs (the red and blue curves), the zero-bias *G* shows a continuous decrease as increasing *T*, consistent with the observation in Fig. 3. For large ZBPs (the orange and green curves), the zero-bias *G* initially increases and then decreases as increasing *T*, consistent with the observation in Fig. 2. Figure 4 is for illustration purposes and a qualitative comparison. A quantitative theoretical fitting is provided in Fig. S11 in SM [51].

IV. CONCLUSION

To summarize, we have studied zero-energy ABSs in a weakly dissipative environment. Large ZBPs near $2e^2/h$ can be resolved. The large peak width protects the ZBP height from decreasing against thermal averaging over an intermediate *T* range (e.g., <300 mK) where ECB could dominate. As a result, when *T* is lowered, the ZBP could either decrease its height or split, both not following Fermi-liquid thermal simulation. On the contrary, the *T* dependence of small ZBPs follows the thermal simulation within the current temperature range, which is the same with the cases in regular devices without dissipation. Our result shows that the weak dissipation strength ($R_{film} \sim 2.7$ kΩ) cannot fully suppress ABS-induced ZBPs at the current fridge temperature. For Majorana or quasi-Majorana resonance detection [27,28], a stronger dissipation regime [37] is preferred which can effectively "filter out" trivial ZBPs [36,53–55], since in the weak dissipation regime, the heights of ZBPs induced by zero-energy ABSs could either increase (Fig. 2) or decrease (Fig. 3) as increasing *T*, depending on the ABS details. This makes it less straight-

forward to qualitatively distinguish MZM signatures [56,57] compared to the strong dissipation case.

ACKNOWLEDGMENTS

[1] A. F. Andreev, Thermal conductivity of the intermediate state of superconductors II, Sov. Phys. JETP **19**, 1228 (1964).

[2] A. F. Andreev, Electron spectrum of the intermediate state of superconductors, Sov. Phys. JETP **22**, 18 (1966).

[3] J. Pillet, C. Quay, P. Morfin, C. Bena, A. L. Yeyati, and P. Joyez, Andreev bound states in supercurrent-carrying carbon nanotubes revealed, Nat. Phys. **6**, 965 (2010).

[4] T. Dirks, T. L. Hughes, S. Lal, B. Uchoa, Y.-F. Chen, C. Chialvo, P. M. Goldbart, and N. Mason, Transport through Andreev bound states in a graphene quantum dot, Nat. Phys. **7**, 386 (2011).

[5] W. Chang, V. E. Manucharyan, T. S. Jespersen, J. Nygård, and C. M. Marcus, Tunneling Spectroscopy of Quasiparticle Bound States in a Spinful Josephson Junction, Phys. Rev. Lett. **110**, 217005 (2013).

[6] Y. Jiang, S. Yang, L. Li, W. Song, W. Miao, B. Tong, Z. Geng, Y. Gao, R. Li, F. Chen, Q. Zhang, F. Meng, L. Gu, K. Zhu, Y. Zang, R. Shang, Z. Cao, X. Feng, Q.-K. Xue, D. E. Liu *et al.*, Selective area epitaxy of PbTe-Pb hybrid nanowires on a lattice-matched substrate, Phys. Rev. Mater. **6**, 034205 (2022).

[7] J. A. van Dam, Y. V. Nazarov, E. P. Bakkers, S. De Franceschi, and L. P. Kouwenhoven, Supercurrent reversal in quantum dots, Nature (London) **442**, 667 (2006).

[8] E. J. Lee, X. Jiang, M. Houzet, R. Aguado, C. M. Lieber, and S. De Franceschi, Spin-resolved Andreev levels and parity crossings in hybrid superconductor–semiconductor nanostructures, Nat. Nanotechnol. **9**, 79 (2014).

[9] H. Zhang, Ö. Gül, S. Conesa-Boj, M. P. Nowak, M. Wimmer, K. Zuo, V. Mourik, F. K. De Vries, J. Van Veen, M. W. De Moor *et al.*, Ballistic superconductivity in semiconductor nanowires, Nat. Commun. **8**, 16025 (2017).

[10] M. W. A. de Moor, J. D. S. Bommer, D. Xu, G. W. Winkler, A. E. Antipov, A. Bargerbos, G. Wang, N. van Loo, R. L. M. Op het Veld, S. Gazibegovic *et al.*, Electric field tunable superconductor-semiconductor coupling in Majorana nanowires, New J. Phys. **20**, 103049 (2018).

[11] J. D. S. Bommer, H. Zhang, Ö. Gül, B. Nijholt, M. Wimmer, F. N. Rybakov, J. Garaud, D. Rodic, E. Babaev, M. Troyer, D. Car, S. R. Plissard, E. P. A. M. Bakkers, K. Watanabe, T. Taniguchi, and L. P. Kouwenhoven, Spin-Orbit Protection of Induced Superconductivity in Majorana Nanowires, Phys. Rev. Lett. **122**, 187702 (2019).

[12] C. Jünger, R. Delagrange, D. Chevallier, S. Lehmann, K. A. Dick, C. Thelander, J. Klinovaja, D. Loss, A. Baumgartner, and C. Schönenberger, Magnetic-Field-Independent Subgap States in Hybrid Rashba Nanowires, Phys. Rev. Lett. **125**, 017701 (2020).

[13] R. M. Lutchyn, J. D. Sau, and S. Das Sarma, Majorana Fermions and a Topological Phase Transition in Semiconductor-Superconductor Heterostructures, Phys. Rev. Lett. **105**, 077001 (2010).

[14] Y. Oreg, G. Refael, and F. von Oppen, Helical Liquids and Majorana Bound States in Quantum Wires, Phys. Rev. Lett. **105**, 177002 (2010).

[15] V. Mourik, K. Zuo, S. M. Frolov, S. Plissard, E. P. Bakkers, and L. P. Kouwenhoven, Signatures of Majorana fermions in hybrid superconductor-semiconductor nanowire devices, Science **336**, 1003 (2012).

[16] M. Deng, S. Vaitiekėnas, E. B. Hansen, J. Danon, M. Leijnse, K. Flensberg, J. Nygård, P. Krogstrup, and C. M. Marcus, Majorana bound state in a coupled quantum-dot hybrid-nanowire system, Science **354**, 1557 (2016).

[17] Ö. Gül, H. Zhang, J. D. Bommer, M. W. de Moor, D. Car, S. R. Plissard, E. P. Bakkers, A. Geresdi, K. Watanabe, T. Taniguchi *et al.*, Ballistic Majorana nanowire devices, Nat. Nanotechnol. **13**, 192 (2018).

[18] H. Zhang, M. W. de Moor, J. D. Bommer, D. Xu, G. Wang, N. van Loo, C.-X. Liu, S. Gazibegovic, J. A. Logan, D. Car, R. L. M. Op het Veld, P. J. van Veldhoven, S. Koellinga, M. A. Verheijen, M. Pendharkar, D. J. Pennachio, B. Shojaei, J. S. Lee, C. J. Palmstrøm, E. P. Bakkers *et al.*, Large zero-bias peaks in InSb-Al hybrid semiconductor-superconductor nanowire devices, arXiv:2101.11456.

[19] H. Song, Z. Zhang, D. Pan, D. Liu, Z. Wang, Z. Cao, L. Liu, L. Wen, D. Liao, R. Zhuo, D. E. Liu, R. Shang, J. Zhao, and H. Zhang, Large zero bias peaks and dips in a four-terminal thin InAs-Al nanowire device, Phys. Rev. Res. **4**, 033235 (2022).

[20] Z. Wang, H. Song, D. Pan, Z. Zhang, W. Miao, R. Li, Z. Cao, G. Zhang, L. Liu, L. Wen, R. Zhuo, D. E. Liu, K. He, R. Shang, J. Zhao, and H. Zhang, Plateau Regions for Zero-Bias Peaks within 5% of the Quantized Conductance Value $2e^2/h$, Phys. Rev. Lett. **129**, 167702 (2022).

[21] H. Zhang, D. E. Liu, M. Wimmer, and L. P. Kouwenhoven, Next steps of quantum transport in Majorana nanowire devices, Nat. Commun. **10**, 5128 (2019).

[22] E. Prada, P. San-Jose, M. W. de Moor, A. Geresdi, E. J. Lee, J. Klinovaja, D. Loss, J. Nygård, R. Aguado, and L. P. Kouwenhoven, From Andreev to Majorana bound states in hybrid superconductor–semiconductor nanowires, Nat. Rev. Phys. **2**, 575 (2020).

[23] E. Prada, P. San-Jose, and R. Aguado, Transport spectroscopy of NS nanowire junctions with Majorana fermions, Phys. Rev. B **86**, 180503(R) (2012).

[24] J. Liu, A. C. Potter, K. T. Law, and P. A. Lee, Zero-Bias Peaks in the Tunneling Conductance of Spin-Orbit-Coupled

Superconducting Wires with and without Majorana End-States, Phys. Rev. Lett. **109**, 267002 (2012).

[25] G. Kells, D. Meidan, and P. W. Brouwer, Near-zero-energy end states in topologically trivial spin-orbit coupled superconducting nanowires with a smooth confinement, Phys. Rev. B **86**, 100503(R) (2012).

[26] C.-X. Liu, J. D. Sau, T. D. Stanescu, and S. Das Sarma, Andreev bound states versus Majorana bound states in quantum dot-nanowire-superconductor hybrid structures: Trivial versus topological zero-bias conductance peaks, Phys. Rev. B **96**, 075161 (2017).

[27] C. Moore, C. Zeng, T. D. Stanescu, and S. Tewari, Quantized zero-bias conductance plateau in semiconductor-superconductor heterostructures without topological Majorana zero modes, Phys. Rev. B **98**, 155314 (2018).

[28] A. Vuik, B. Nijholt, A. Akhmerov, and M. Wimmer, Reproducing topological properties with quasi-Majorana states, SciPost Phys. **7**, 061 (2019).

[29] D. E. Liu, E. Rossi, and R. M. Lutchyn, Impurity-induced states in superconducting heterostructures, Phys. Rev. B **97**, 161408(R) (2018).

[30] Z. Cao, H. Zhang, H.-F. Lü, W.-X. He, H.-Z. Lu, and X. C. Xie, Decays of Majorana or Andreev Oscillations Induced by Steplike Spin-Orbit Coupling, Phys. Rev. Lett. **122**, 147701 (2019).

[31] C. Reeg, O. Dmytruk, D. Chevallier, D. Loss, and J. Klinovaja, Zero-energy Andreev bound states from quantum dots in proximitized Rashba nanowires, Phys. Rev. B **98**, 245407 (2018).

[32] H. Pan and S. Das Sarma, Physical mechanisms for zero-bias conductance peaks in Majorana nanowires, Phys. Rev. Res. **2**, 013377 (2020).

[33] S. Das Sarma and H. Pan, Disorder-induced zero-bias peaks in Majorana nanowires, Phys. Rev. B **103**, 195158 (2021).

[34] C. Zeng, G. Sharma, S. Tewari, and T. Stanescu, Partially separated Majorana modes in a disordered medium, Phys. Rev. B **105**, 205122 (2022).

[35] D. Liu, Z. Cao, X. Liu, H. Zhang, and D. E. Liu, Topological Kondo device for distinguishing quasi-Majorana and Majorana signatures, Phys. Rev. B **104**, 205125 (2021).

[36] D. E. Liu, Proposed Method for Tunneling Spectroscopy with Ohmic Dissipation Using Resistive Electrodes: A Possible Majorana Filter, Phys. Rev. Lett. **111**, 207003 (2013).

[37] S. Zhang, Z. Wang, D. Pan, H. Li, S. Lu, Z. Li, G. Zhang, D. Liu, Z. Cao, L. Liu, L. Wen, D. Liao, R. Zhuo, R. Shang, D. E. Liu, J. Zhao, and H. Zhang, Suppressing Andreev Bound State Zero Bias Peaks Using a Strongly Dissipative Lead, Phys. Rev. Lett. **128**, 076803 (2022).

[38] P. Delsing, K. K. Likharev, L. S. Kuzmin, and T. Claeson, Effect of high-frequency electrodynamic environment on the single-electron tunneling in ultrasmall junctions, Phys. Rev. Lett. **63**, 1180 (1989).

[39] G. L. Ingold and Y. V. Nazarov, *Single Charge Tunnelling: Coulomb Blockade Phenomena in Nanostructures*, edited by H. Grabert and M. H. Devoret (Springer, New York, 1992), pp. 21–107.

[40] K. Flensberg, S. M. Girvin, M. Jonson, D. R. Penn, and M. D. Stiles, Quantum mechanics of the electromagnetic environment in the single-junction Coulomb blockade, Phys. Scr. T **42**, 189 (1992).

[41] P. Joyez, D. Esteve, and M. H. Devoret, How Is the Coulomb Blockade Suppressed in High-Conductance Tunnel Junctions? Phys. Rev. Lett. **80**, 1956 (1998).

[42] W. Zheng, J. Friedman, D. Averin, S. Han, and J. Lukens, Observation of strong Coulomb blockade in resistively isolated tunnel junctions, Solid State Commun. **108**, 839 (1998).

[43] F. Parmentier, A. Anthore, S. Jezouin, H. Le Sueur, U. Gennser, A. Cavanna, D. Mailly, and F. Pierre, Strong back-action of a linear circuit on a single electronic quantum channel, Nat. Phys. **7**, 935 (2011).

[44] H. T. Mebrahtu, I. V. Borzenets, D. E. Liu, H. Zheng, Y. V. Bomze, A. I. Smirnov, H. U. Baranger, and G. Finkelstein, Quantum phase transition in a resonant level coupled to interacting leads, Nature (London) **488**, 61 (2012).

[45] H. Mebrahtu, I. Borzenets, H. Zheng, Y. V. Bomze, A. Smirnov, S. Florens, H. Baranger, and G. Finkelstein, Observation of Majorana quantum critical behaviour in a resonant level coupled to a dissipative environment, Nat. Phys. **9**, 732 (2013).

[46] D. E. Liu, H. Zheng, G. Finkelstein, and H. U. Baranger, Tunable quantum phase transitions in a resonant level coupled to two dissipative baths, Phys. Rev. B **89**, 085116 (2014).

[47] S. Jezouin, M. Albert, F. Parmentier, A. Anthore, U. Gennser, A. Cavanna, I. Safi, and F. Pierre, Tomonaga–Luttinger physics in electronic quantum circuits, Nat. Commun. **4**, 1802 (2013).

[48] A. Anthore, Z. Iftikhar, E. Boulat, F. D. Parmentier, A. Cavanna, A. Ouerghi, U. Gennser, and F. Pierre, Circuit Quantum Simulation of a Tomonaga-Luttinger Liquid with an Impurity, Phys. Rev. X **8**, 031075 (2018).

[49] K. Wölms and K. Flensberg, Environmental coulomb blockade of topological superconductor-normal metal junctions, Phys. Rev. B **92**, 165428 (2015).

[50] I. Safi and H. Saleur, One-Channel Conductor in an Ohmic Environment: Mapping to a Tomonaga-Luttinger Liquid and Full Counting Statistics, Phys. Rev. Lett. **93**, 126602 (2004).

[51] See Supplemental Material at http://link.aps.org/supplemental/10.1103/PhysRevB.106.205421 for additional data and analysis.

[52] D. Pan, H. Song, S. Zhang, L. Liu, L. Wen, D. Liao, R. Zhuo, Z. Wang, Z. Zhang, S. Yang, J. Ying, W. Miao, R. Shang, H. Zhang, and J. Zhao, *In situ* epitaxy of pure phase ultra-thin InAs-Al nanowires for quantum devices, Chin. Phys. Lett. **39**, 058101 (2022).

[53] D. Liu, G. Zhang, Z. Cao, H. Zhang, and D. E. Liu, Universal Conductance Scaling of Andreev Reflections Using a Dissipative Probe, Phys. Rev. Lett. **128**, 076802 (2022).

[54] G. Zhang and C. Spånslätt, Distinguishing between topological and quasi Majorana zero modes with a dissipative resonant level, Phys. Rev. B **102**, 045111 (2020).

[55] D. Liu, Z. Cao, H. Zhang, and D. E. Liu, Revealing the nonlocal coherent nature of Majorana devices from dissipative teleportation, Phys. Rev. B **101**, 081406(R) (2020).

[56] K. Sengupta, I. Žutić, H.-J. Kwon, V. M. Yakovenko, and S. Das Sarma, Midgap edge states and pairing symmetry of quasi-one-dimensional organic superconductors, Phys. Rev. B **63**, 144531 (2001).

[57] K. T. Law, P. A. Lee, and T. K. Ng, Majorana Fermion Induced Resonant Andreev Reflection, Phys. Rev. Lett. **103**, 237001 (2009).

[58] https://doi.org/10.5281/zenodo.7351074.